# Extended abstracts from the SME journal Mining, Metallurgy & Exploration

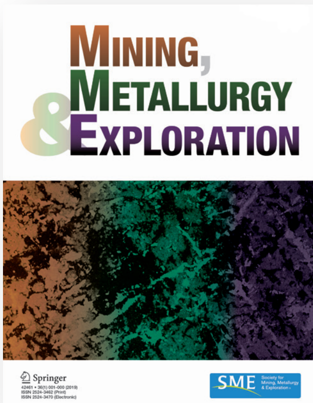


Take full advantage of your SME membership. As a member, you can read and download for free all of the full-text papers in *Mining, Metallurgy & Exploration* (**MME**) and the archives of *Minerals & Metallurgical Processing* (**MMP**). Log in to the SME website as a member, and enter the MME Springer website through our dedicated SME link:

1. Log in at smenet.org with your email address and password.
2. Click on "Publications" in the top banner and choose "Mining, Metallurgy & Exploration journal" in the pull-down menu.
3. Scroll down and click on the "Read the MME Journal Online" link. This takes you to the MME Springer website as an SME member with free access.

To see a specific paper, use the search function or the paper's https://doi link.

For assistance anytime, email Chee Theng at theng@smenet.org. ■

**IMPACT FACTOR 2.0**

**Submit your paper by clicking on the "Submit manuscript" box at springer.com/42461**
**Get Table of Contents (ToC) email alerts by clicking on "Sign up for alerts"**

**MME is abstracted and indexed in Web of Science, Current Contents, Science Citation Index Expanded, Scopus, Google Scholar, EBSCO, ProQuest and more.**



## Invited Extended Abstracts

## Evaluating the feasibility of incorporating fuel-cell drive trains into existing haul trucks

**Ayorinde Akinrinlola, Kwame Awuah-Offei*and Abdullah Al Moinee**
Department of Mining & Explosives Engineering, Thomas J. O'Keefe Institute for Sustainable Supply of Strategic Minerals,
Missouri University of Science & Technology, Rolla, MO, USA
*Corresponding author email: kwamea@mst.edu

**Full-text paper:**
Mining, Metallurgy & Exploration (2025) 42:3405–3423, https://doi.org/10.1007/s42461-025-01361-7

**Keywords:** Mine haulage, Haul trucks, Fuel cell, Drive train modeling, Renewable energy



*Hydrogen fuel cells have emerged as a critical technology for the mining industry to meet promising carbon reduction targets in material handling. This work evaluates the practical challenges of transitioning from diesel to hydrogen by simulating the energy demands of a Komatsu 830-E haul truck across various duty cycles. Our findings reveal a significant volumetric gap: while a short-haul cycle consumes only 23.6 L of diesel, it requires more than 17,700 L of hydrogen at standard temperature and pressure. Even when compressed to 700 bars, the storage and fuel cell components exceed the available chassis space of current truck form factors. Consequently, achieving the same driving range as diesel through retrofitting is currently unfeasible, signaling that the industry's shift to hydrogen will require a fundamental redesign of vehicle architectures by original equipment manufacturers and substantial investment in specialized onsite infrastructure.*

### Background

Decarbonization has emerged as a paramount challenge for the mining sector, which is responsible for 4 to 7 percent of global greenhouse-gas (GHG) emissions [1]. A significant portion of these emissions—ranging from 30 to 80 percent at individual sites — stems from material handling operations reliant on diesel-powered haul trucks [2]. While battery-electric vehicles and trolley-assist systems are current alternatives, they are often limited by low energy density, extended charging requirements and the carbon intensity of local electrical grids [3,4]. Hydrogen fuel cells offer a compelling solution that can provide onboard clean energy generation with zero tailpipe emissions and refueling times comparable to diesel. However, the rapid deployment of this technology likely hinges on retrofitting existing truck architectures

[5]. This study addresses a critical gap in the literature by evaluating and modeling whether the real estate of current diesel-electric haul trucks can realistically accommodate the fuel-cell stacks and high-pressure hydrogen storage required to maintain existing productivity and range.

## Methodology

To assess the feasibility of retrofitting, we developed a vehicle drivetrain and energy simulation model in MATLAB/Simulink. The model uses the Komatsu 830E-5 diesel-electric truck (see the full paper for key specifications of the truck) as a reference, utilizing field-derived drive cycle data (velocity, weight and inclination) from actual mining operations to ensure realistic power demands [6]. The simulation framework consists of three integrated subsystems:

1. Driver submodel: This system functions as a proportional-integral (PI) controller that compares desired field velocity with simulated feedback to generate acceleration and braking commands, ensuring the virtual truck adheres to real-world duty cycles.
2. Powertrain submodel (Fig. 1a): This subsystem models the motor, inverter and a hybrid energy management system (EMS). Following the architecture of existing fuel-cell vehicles, we utilized a fuel-cell stack as the primary power source and a 100-kWh battery for auxiliary power and regenerative braking. The EMS logic dictates that the battery handles power requests up to 200 kW and captures energy during braking, while the fuel cell meets all demands exceeding that threshold.
3. Vehicle dynamics submodel (Fig. 1b): This component calculates the total tractive force required by subtracting resistive forces from the powertrain's output. The model accounts for aerodynamic drag, grade resistance and rolling resistance based on the specific haul road profile.

By integrating these subsystems, the model estimates instantaneous power demand and cumulative hydrogen consumption. The total hydrogen mass required to complete specific cycles was converted into volumetric requirements at storage pressures. These volumes were then compared against the existing "real estate" of the Komatsu 830E-5 to evaluate if a retrofit could achieve a comparable driving range without major structural redesign.

## Results and discussion

Model verification confirmed that the simulated truck precisely followed field velocities for the simulated conditions (ranging from minus 15° to plus 15° grade). The simulation demonstrated a clear volumetric gap between diesel and hydrogen across the three scenarios (Table 1).

**Table 1** — Volume of hydrogen by pressure for all drive cycles.

| | | Drive cycle | | |
|---|---|---|---|---|
| | | Medium (base) (1,100 s) | Short (852 s) | Long (1,551 s) |
| | | Diesel fuel consumed (L) | | |
| | | 29.025 | 23.6 | 82.923 |
| Hydrogen pressure (bar) | Hydrogen density ($kg/m^3$) | Volume of hydrogen (L) | | |
| 1 | 0.09 | 24,081 | 17,729 | 25,705 |
| 350 | 21 | 103.19 | 75.98 | 110.16 |
| 700 | 42 | 51.4 | 37.99 | 55.08 |

Model verification confirmed the simulation precisely follows field velocities, with power draws remaining within the 1,865-kW rated capacity of the Komatsu 830-E. As shown in Fig. 2, the battery and fuel-cell power draws adhere to the hybrid logic, where the battery manages regenerative braking and auxiliary loads while the fuel cell provides primary propulsion. A critical finding is the impact on operational productivity. Our analysis shows that a hydrogen-powered truck would complete only 88 medium-haul cycles before requiring refueling, compared to 156 cycles for an equivalent diesel tank — a 44 percent reduction in range. Furthermore, while the fuel-cell engine itself is spatially efficient ($8.4 \times 10^6$ $cm^3$ versus $28.6 \times 10^6$ $cm^3$ for diesel), the saved space is immediately consumed by 700-bar storage tanks, 1.2-MWh battery packs and thermal management systems.

Managing high-pressure flammable gas near explosives also introduces significant new risk profiles, particularly when operated in proximity to mining explosives. Furthermore, the transition requires a massive investment in onsite infrastructure.

## Conclusion

This study concludes that while hydrogen fuel cells can meet the power demands of heavy-duty haulage, real-estate constraints make simple retrofitting unfeasible. Achieving operational parity — specifically, maintaining the driving range of a 4,542-L diesel tank — requires a storage pres-

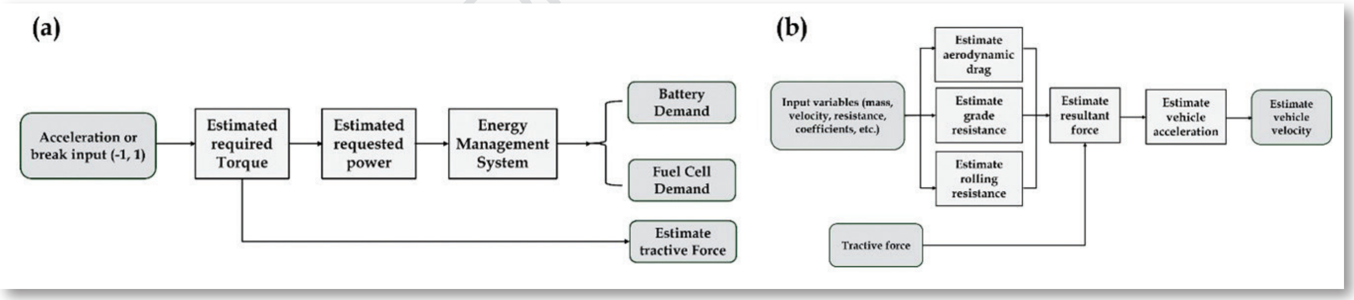


**Fig. 1** Overview of the (a) powertrain submodel and (b) vehicle model.

sure of at least 700 bars, yet the spatial requirements of the full hybrid system exceed existing chassis limits. Consequently, the industry's transition will rely on extensive vehicle redesigns by original equipment manufacturers and substantial investment in onsite hydrogen infrastructure. Ultimately, hydrogen remains a promising, though structurally intensive, pillar of the mining industry's zero-emission future. ■

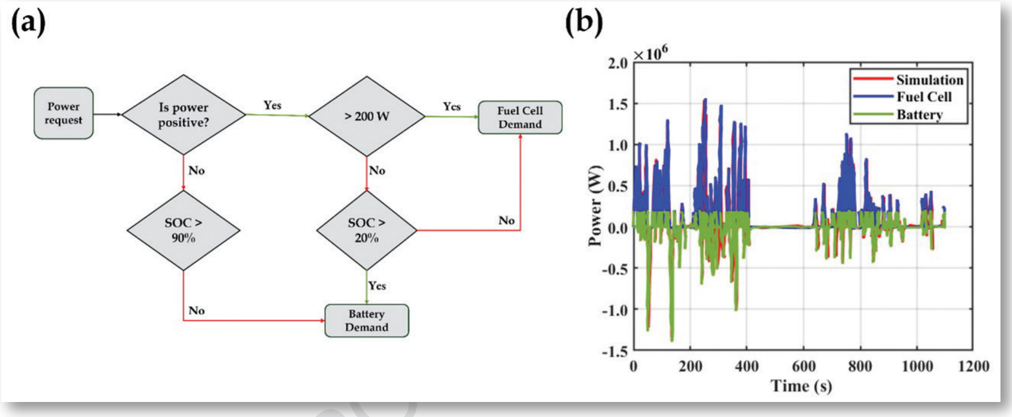


**Fig. 2** (a) Overview of the power distribution algorithm, (b) power requested from simulation, and predicted power for fuel cell and battery.

## Selected references

1. Delevingne L, Glazener W, Grégoir L, Henderson K (2021) Climate risk and decarbonization: What every mining CEO needs to know. McKinsey & Co. Available at: https://www.mckinsey.com/capabilities/sustainability/our-insights/climate-risk-and-decarbonization-what-every-mining-ceo-needs-to-know#/
2. Muralidharan R, Kirk T, Koch Blank T (n.d.) Pulling the weight of heavy truck decarbonization: Exploring pathways to decarbonize bulk material hauling in mining. Available at: https://rmi.org/wp-content/uploads/2019/06/rmi-pulling-the-weight-of-heavy-truck-decarbonization.pdf
3. McGinnis R (2020) $CO_2$-to-fuels renewable gasoline and jet fuel can soon be price competitive with fossil fuels. Joule 4(3):509–511
4. Valenzuela M, Cruzat J (2018) Modeling and evaluation of benefits of trolley assist system for mining trucks. IEEE Trans Ind Appl p 1
5. Durbin DJ, Malardier-Jugroot C (2013) Review of hydrogen storage techniques for on board vehicle applications. Int J Hydrogen Energy 38(34):14595–14617
6. Komatsu America Corp (2019) Komatsu 830E-5 brochure pp 1–20. Available at: https://www.smsequipment.com/getmedia/c0aac900-44bb-49ca-bdbc-d1ceaf37604e/830E-5.pdf

# Geophysical and geochemical data of mineral resources with an emphasis on gold and associated minerals in Atshan area in south Eastern Desert, Egypt

**Sultan A.S. Araffa[1,*], Mahdy Kh Abd-Elsadek[2], Mohamed Aldeep[1], Hazem Badreldin[1,4], Adel A.A. Othman[3], Waheed H. Mohamed[3] and Khaled Zaghlol[1]**

[1]National Research Institute of Astronomy and Geophysics (NRIAG), Helwan, Cairo, Egypt
[2]Egyptian Mineral Resources Authority (EMRA), Cairo, Egypt
[3]Geology Department, Faculty of Science, Al-Azhar University, Egypt
[4]National Institute of Oceanography and Applied Geophysics, Udine, Italy
*Corresponding author email: sultan_awad@yahoo.com

**Full-text paper:**
Mining, Metallurgy & Exploration (2026) 43:463–481, https://doi.org/10.1007/s42461-025-01432-9

**Keywords:** Gold mineralization, Atshan area, Ground magnetic, Resistivity, Chargeability

*This research provides a validated, data-driven exploration model for gold and associated sulfide mineralization in the Atshan area in south Eastern Desert in Egypt. By integrating high-resolution ground geophysical surveys with geochemical and geological data, the study successfully delineates shallow (5 to 40 m) mineralized bodies controlled by a complex shear zone system. In a real-world context, this methodology offers a high-precision blueprint for mining exploration in the Arabian-Nubian Shield, significantly reducing the risk and cost of drilling campaigns by accurately targeting subsurface ore bodies through noninvasive techniques.*

## Background

The Arabian-Nubian Shield is a prolific neoproterozoic tectonic province, renowned for hosting gold and base-metal deposits that have been mined since pharaonic times. Within the south Eastern Desert of Egypt, mineralization is primarily structurally controlled, typically occurring in shear zones, quartz veins and hydrothermally altered rocks. The Atshan area, located southwest of Marsa Alam, is situated within the prospective Hamata district. Despite previous regional studies, localized exploration in Atshan has been limited by insufficient geophysical resolution and a lack of integrated structural reanalysis. This study addresses these gaps by synthesizing geological mapping, geochemical analysis and ground geophysics to characterize the subsurface architecture and identify high-priority gold targets.

## Methods

The study employed an integrated approach to charac-

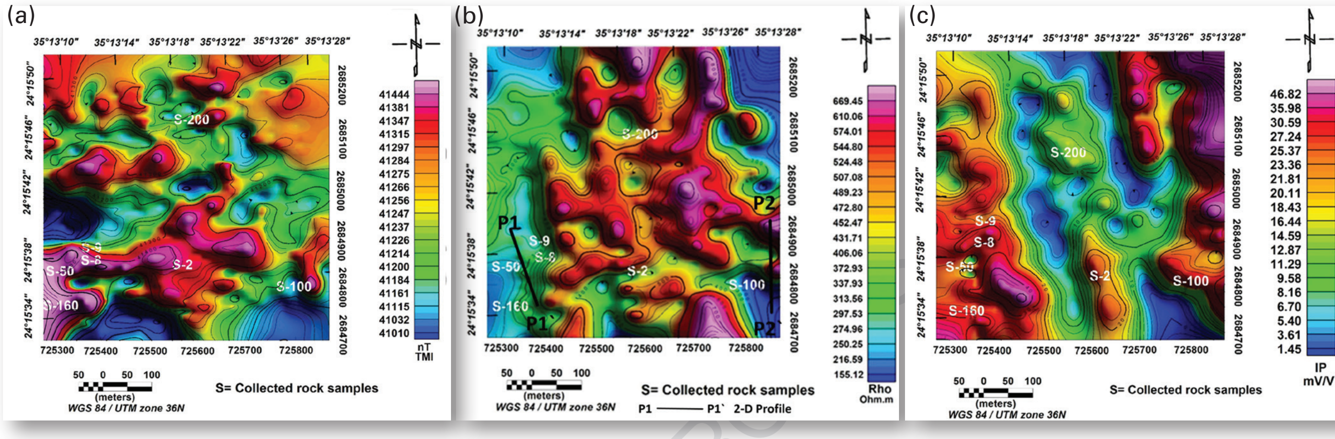


**Fig. 1** Integration of (a) total magnetic intensity, (b) true resistivity and (c) induced polarization maps showing the spatial correlation with mineralized zones.

terize the mineral potential of the Atshan area.

- Geological mapping: Field verification was conducted to describe rock units, including island-arc metavolcanics (80 percent of the area), granodiorites and intrusive dikes.
- Geochemical analysis: Rock samples were collected from alteration zones and quartz veins. Gold (Ag) and associated element concentrations — copper (Cu), lead (Pb), zinc (Zn) — were determined using atomic absorption.

## Geophysical survey

- Magnetic survey: Measurements were taken at 550 stations along 11 profiles to identify structural trends and magnetic anomalies. Advanced processing included total magnetic intensity (TMI) and source parameter imaging (SPI).

## Geoelectrical survey

- Direct-current (DC) resistivity and induced-polarization (IP) data were simultaneously collected using a gradient array with 5-m electrode spacing.
- Two-dimensional (2D) imaging: Wenner-Schlumberger array profiles were conducted to generate vertical cross-sections of the subsurface.

## Results

Integration of the data sets revealed a strong spatial correlation between geophysical signatures and chemical anomalies.

**Geochemical signatures.** Multiple gold anomalies were identified, with peak concentrations reaching 7.8 ppm. These zones were also highly enriched in copper (up to 13,624 ppm) and lead (up to 12,040 ppm).

*Magnetic patterns.* High-amplitude anomalies (greater than 41,440 nT) were identified in the southwestern, southeastern and central regions. These correspond to altered metavolcanic rocks.

*Electrical signatures.* Zones of low resistivity (less than 200 ohm·m) and high chargeability (up to 52 ms) indicated disseminated sulfide mineralization containing encapsulated gold.

*Depth estimates.* SPI and power-spectrum analyses estimated mineralized bodies at depths of 5 to 40 m.

## Discussion

The mineralization in Atshan is conclusively structurally controlled. The primary conduits for mineralizing fluids were an E-W trending shear zone and the NE-SW trending southern extension of the Hafafit shear zone. The convergence of these structural lineaments created zones of enhanced permeability, leading to the deposition of sulfides and gold in stockworks and quartz veins.

The geophysical expression — specifically, the coincidence of magnetic highs, low resistivity and high chargeability — accurately maps the hydrothermal alteration and sulfide accumu-

**Table 1** — Types, coordinates and results of atomic absorption analyses of gold and associated elements of bedrock samples in the prospecting area.

| S No. | X | Y | Au (ppm) | Ag (ppm) | Cu (ppm) | Pb (ppm) | Zn (ppm) | Notes |
|---|---|---|---|---|---|---|---|---|
| S–8 | 725400 | 2684863 | 0.6 | 1.5 | 6.1 | – | – | |
| S–9 | 725410 | 2684900 | 0.3 | 0.6 | 44.3 | – | – | |
| S–2 | 725600 | 2684840 | 0.42 | 3.1 | 21.42 | 400 | 2066 | Alter. zone |
| S–100 | 725850 | 2684840 | 0.6 | 1.1 | 17.3 | 18 | 119.5 | |
| S–200 | 725600 | 2685100 | 0.6 | 0.6 | 3 | 33.7 | 206.3 | |
| S–50 | 725380 | 2684820 | 2.82 | 1.52 | 8080 | 114.43 | 2160 | Atshan mine (Alter. zone) |
| S–160 | 725360 | 2684800 | 7.8 | 0.8 | 13624 | 12040 | 951 | |
| Detection limits | | | 0.03 | 0.06 | 0.05 | 0.1 | 0.005 | |

lation. The two-dimensional vertical sections (Figs. 1 and 2) further suggest that mineralization is not confined to a single horizon but occurs as multiple subvertical bodies, supporting a vein-type exploration model.

## Conclusions

The integrated methodology successfully identified high-priority targets in the western, central and southeastern sectors of Atshan. The study confirms that gold is encapsulated within sulfide minerals hosted in sheared intermediate metavolcanic rocks. Given the shallow nature of the identified anomalies (5 to 40 m), immediate systematic drilling is recommended to evaluate the economic grade and resource continuity of these targets. ■

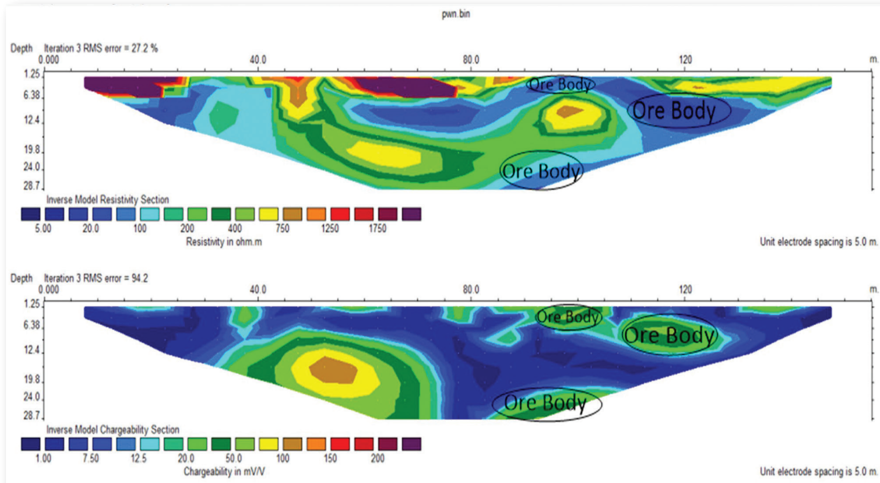


**Fig. 2** 2D Wenner-Schlumberger inversions for profile P1, illustrating subsurface orebodies as high chargeability/low resistivity zones.


## Selected references

1. Sultan SA, Mansour SA, Santos FM, Helaly AS (2009) Geophysical exploration for gold and associated minerals at Wadi El Beida Area, South-eastern Desert, Egypt, Journal of Geophysics and Engineering 6:345–356
2. Zoheir BA, Emam A (2012) Application of ASTER data to lithological mapping and ore mineral exploration: Case study from the Fawakhir area, Eastern Desert of Egypt, Arab J Geosci 5(5):1055–1068
3. Horo D, Pal SK, Singh S (2021) Mapping of gold mineralization in Ichadih, North Singhbhum Mobile Belt, India using electrical resistivity tomography and self-potential methods. Min Metall Explor 38:397–411
4. Abdel-Karim A-AM (2022) Genesis of sulfide mineralization, Atshan and Darhib areas, south Eastern Desert of Egypt: Evidence of fluid pathway effects along shear zones. Arab J Sci Eng. 47:641–665


Collection on Health and Safety in Mining

# Use of ultrasonic water spray systems for respirable coal mine dust control in underground coal mines


**Maria Beltran-Marquez[1], Sina Siahidouzazar[2], Mohammad Rezaee[3] and Pedram Roghanchi[2,*]**

[1]Department of Mineral Engineering, New Mexico Institute of Mining and Technology, Socorro, NM, USA
[2]Department of Mining Engineering, University of Kentucky, Lexington, KY, USA
[3]Department of Energy and Mineral Engineering, Pennsylvania State University, State College, PA, USA
*Corresponding author email: pedram.roghanchi@uky.edu



**Full-text paper:**
Mining, Metallurgy & Exploration (2026) 43:711–726, https://doi.org/10.1007/s42461-025-01401-2

**Keywords:** Respirable coal mine dust (RCMD), Ultrasonic nozzles, Air-atomizing nozzles, Dust control, Droplets



*Respirable coal mine dust (RCMD) remains one of the most persistent hazards in underground coal mining because the smallest particles stay airborne longer, are harder to capture, and contribute to chronic lung disease risk. Conventional water sprays are widely used, but they are less effective against very fine coal dust because coal is hydrophobic and large droplets often let fine particles move around them with the airflow instead of colliding. This study shows that ultrasonic nozzles, which generate much finer droplets than conventional air-atomizing sprays, can improve airborne dust capture under controlled ventilation conditions representative of underground mines. In the tested configuration, ultrasonic nozzles reduced respirable dust by roughly 20 to 30 percent more than the air-atomizing nozzles, suggesting they could strengthen layered mine dust-control programs where ultra-fine dust is especially difficult to suppress.*


## Background

RCMD is generated during routine mining activities and remains a major occupational health and safety concern. Long-term exposure is linked to pulmonary disease, including coal workers' pneumoconiosis, and excessive airborne coal dust can also contribute to explosion hazards. Although water sprays are popular because they are relatively simple and economical, many dust-control systems still remove only a portion of the airborne dust load in mine environments.

One reason is that conventional sprays often produce droplets much larger than respirable dust particles. When droplet and particle sizes are poorly matched, the dust follows air streamlines around the droplets rather than attaching to them. This study focuses on whether ultrasonic atomization, which can produce much finer droplets and keep them suspended longer, offers an advantage for capturing the respirable fraction.

## Methods

The study was conducted in a laboratory wind tunnel designed to simulate underground mine ventilation. Coal dust from the Northern Appalachian region was aerosolized and introduced into the tunnel, where five nozzles were tested: three ultrasonic nozzles (SK508, SV882 and SV980) and two air-atomizing nozzles (SU22 and SU11). Test conditions were first standardized to produce a stable dust environment, and the selected settings generated dust concentrations of about 1.5 to 2.0 mg/m$^3$. Surfactants were added to the water to improve droplet-particle interaction. Because preliminary testing showed that the PDM3700 also detected water droplets and could misclassify them as dust, each nozzle was evaluated in a three-stage, 20-min protocol: dust-only to establish the baseline dust concentration and particle size distribution, dust-plus-water to measure system response with the spray active, and water-only to quantify the instrument signal caused by droplets alone. This design allowed the study to separate true dust suppression from measurement artifact caused by airborne spray droplets. The operating conditions for the tested nozzles are summarized in Table 1, and the wind-tunnel configuration used to generate and monitor the aerosolized dust stream is shown in Fig. 1.

## Results and discussion

The particle size distribution showed that the test atmosphere was dominated by ultrafine respirable dust. Across

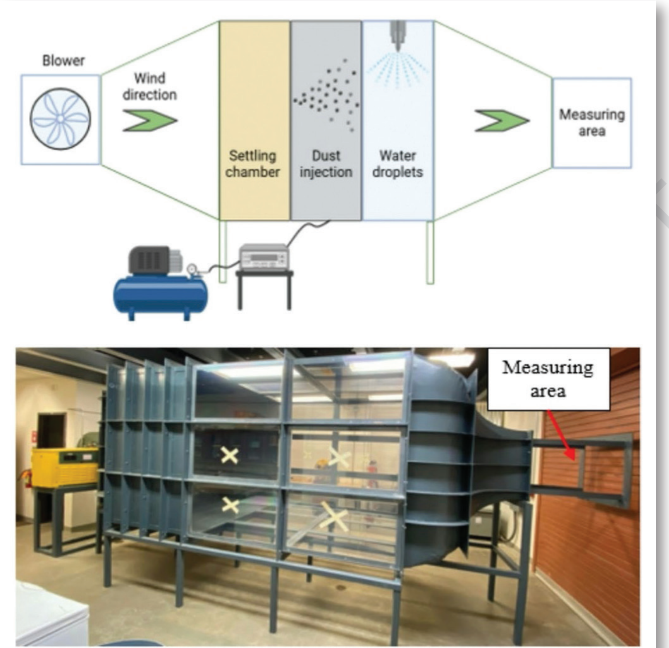


**Fig. 1** Wind tunnel setup for the experiment.

**Table 1** — Nozzle working parameters.

| Type of nozzle | Model | Air pressure (kPa) | Water pressure (kPa) |
|---|---|---|---|
| Atomizing | ¼ J with SU22B setup | 193 | 138 |
| | ¼ J with SU11 setup | 193 | 138 |
| Ultrasonic | SK508 | 500 | 100 |
| | SV882 | 500 | 100 |
| | SV980 | 500 | 50 |



experiments, the mean aerodynamic diameter was about 1.46 μm, 99 percent of particles were smaller than 6 μm, and more than 85 percent were smaller than 2 μm. This is important because these are the particles that are difficult to suppress with conventional sprays. A representative particle size distribution is shown in Fig. 2.

The ultrasonic nozzles outperformed the air-atomizing nozzles. The best-performing nozzle was SK508, with an average dust reduction of 67 percent. The other two ultrasonic nozzles, SV980 and SV882, produced similar average reductions of 56 percent and 55 percent, respectively. By comparison, the air-atomizing nozzles performed below 50 percent overall, and the SU11 showed especially weak atomization during testing. Statistical analysis supported these trends: Analysis of variance (ANOVA) showed that ultrasonic nozzles performed significantly better than air-atomizing nozzles ($p = 0.002$; Table 2), and that SK508 also differed significantly from the other ultrasonic models.

The performance difference is consistent with the study's physical interpretation of dust capture. Ultrasonic sprays generate fine droplets that more closely match the respirable fraction and can remain suspended long enough to increase droplet-dust interaction. But droplet size alone does not explain performance. Spray angle, coverage volume, induced airflow, droplet-size distribution and local flow structure all influence whether droplets contact dust-laden air. That is why SK508 likely performed better than the other ultrasonic nozzles: not simply because it was "finer," but because its overall spray behavior better supported capture under the

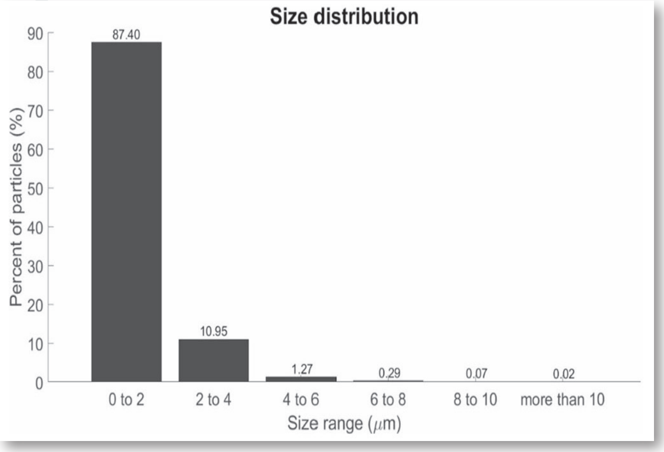


**Fig. 2** Representative particle size distribution from the experiments.

tested conditions.

The practical concerns that matter for mine use include that fine droplets may remain airborne, increase humidity or impose additional ventilation demands, and ultrasonic systems may be sensitive to fouling and maintenance in dust-rich environments. For that reason, ultrasonic sprays are a promising supplemental control for ultrafine RCMD, not as a standalone replacement for broader mine dust-control systems.

## Conclusion

This study demonstrates that ultrasonic water sprays can outperform conventional air-atomizing nozzles for suppressing respirable coal mine dust under controlled ventilation conditions. The advantage was most evident in an atmosphere dominated by ultrafine respirable particles, where the best ultrasonic nozzle achieved substantially higher dust reduction than the air-atomizing alternatives. For mine operators, the practical takeaway is that ultrasonic atomization may be a useful addition to integrated dust-control programs, especially where controlling the finest airborne dust is a priority. Future work should evaluate these systems under a wider range of mine ventilation conditions and address long-term operational issues such as droplet persistence, maintenance and field durability.

**Table 2** — ANOVA results for nozzle types (ultrasonic versus air-atomizing).

| Source | DF | Adj. SS | Adj. MS | F-value | P-value |
|---|---|---|---|---|---|
| Type | 1 | 0.9097 | 0.909748 | 16.85 | 0.002 |
| Nozzle (type) | 3 | 0.4743 | 0.158101 | 2.93 | 0.086 |
| Experiment (type, nozzle) | 10 | 0.5398 | 0.053981 | 16.93 | 0.000 |
| Error | 60 | 0.1914 | 0.003189 | | |
| Total | 74 | 2.1152 | | | |

## Acknowledgments

This study was funded by the National Institute for Occupational Safety and Health (NIOSH) under the contract #75D30119C06390.

## References

A list of all references is available in the full paper.

# Vulnerability index-based risk assessment of blast fragmentation: Comparative analysis of RES and ANFIS methodologies

**Chandrakanta Behera*, Subhamoy Ghosh, Tushar Gupta and Manoj Kumar Mishra**
Department of Mining Engineering, National Institute of Technology, Rourkela, India
*Corresponding author emails: 521mn6013@nitrkl.ac.in; chandrakanta1811@gmail.com

**Full-text paper:**
Mining, Metallurgy & Exploration (2026) 43:95–117, https://doi.org/10.1007/s42461-025-01425-8

**Keywords:** Blast fragmentation, Vulnerability index, Rock engineering system (RES), ANFIS, Risk assessment

*Efficient rock fragmentation is essential for improving productivity and reducing operational costs in surface mining. However, predicting fragmentation outcomes remains challenging due to the complex interaction between geological conditions and blast design parameters. This study introduces a vulnerability index (VI)-based rock engineering system (RES) framework for evaluating the risk associated with blast-induced fragmentation and predicting the mean fragment size ($X_{50}$) in surface iron ore mines. The proposed methodology integrates geological parameters such as geological strength index (GSI) and blastability index (BI) with conventional blast design variables to capture the combined influence of rock mass characteristics and blasting practices. The RES-based model also incorporates expert knowledge through an interaction matrix that quantifies relationships between parameters. Results show that the proposed approach successfully identifies fragmentation risk levels and provides a reliable predictive relationship for mean fragment size. The RES model demonstrated significantly better prediction accuracy compared with the adaptive neuro-fuzzy inference system (ANFIS) model. The framework provides mine engineers with a practical tool to evaluate fragmentation risk and optimize blast design.*

## Background

Blasting is a primary method for rock excavation in surface mining operations. The efficiency of blasting largely depends on the resulting rock fragmentation, which directly affects loading, hauling, crushing and grinding processes. Optimal fragmentation reduces energy consumption in comminution circuits and improves overall operational productivity.

Despite decades of research, predicting fragmentation remains difficult due to the highly heterogeneous nature of rock masses and the complex interaction between geological and blasting parameters. Conventional empirical models, such as the Kuz-Ram model, estimate fragmentation based on explosive energy and rock properties. However, these models rely on simplifying assumptions and often fail to adequately account for geological variability.

Rock fragmentation is influenced by three main groups of factors:

1. Rock mass characteristics (such as strength and jointing conditions).
2. Blast design parameters (burden, spacing, stemming

and charge distribution).

3. Explosive properties and energy distribution.

Therefore, a more comprehensive system-based approach is required to analyze these interactions and evaluate the associated risks.

The RES approach analyzes interactions among multiple blasting parameters. In this study, the RES methodology is combined with a VI concept to assess fragmentation risk and predict the mean fragment size produced by blasting operations.

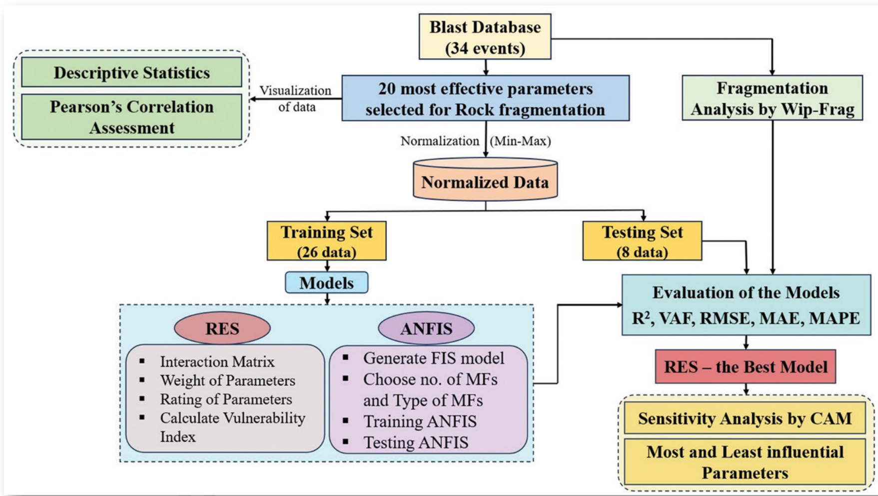


**Fig. 1** Research methodology and workflow.

## Methodology

Field data used in this study were collected from an operating iron ore mine located in eastern India. A total of 34 blast events were recorded, from which 26 blasts were used to develop the predictive model and eight blasts were used for independent validation (Fig. 1).

Twenty parameters influencing blast fragmentation were considered in the analysis. These included blast design parameters such as burden, spacing, hole depth, bench height, powder factor, charge per hole, maximum charge per delay and stemming height.

Geological parameters such as GSI and BI were also incorporated to represent rock mass characteristics.

Fragmentation outcomes were quantified using the mean fragment size ($X_{50}$) obtained through digital image analysis of muck piles. High-resolution images of blasted material were processed using WipFrag image analysis software, which generated particle size distribution curves for each blast. The $X_{50}$ value derived from these curves served as the primary indicator of fragmentation performance.

To compare predictive performance, an adaptive neuro-fuzzy inference system (ANFIS) model was also developed. ANFIS combines neural networks and fuzzy logic to model nonlinear relationships. The model was trained using 26 blast data sets and validated using the remaining eight blasts.

The RES model was constructed using an interaction matrix, which represents the relationships between different parameters influencing fragmentation. Interactions were quantified using the expert semiquantitative (ESQ) approach, assigning influence levels from 0 (no influence) to 4 (critical influence). From this matrix, cause-and-effect relationships between parameters were calculated to determine their relative weights in the system.

These weights were then used to compute the VI for each blast event. The VI represents the likelihood of unfavorable fragmentation outcomes and ranges from 0 to 100. Based on this scale, blasts can be categorized into three risk levels: (1) low-medium risk, (2) medium-high risk and (3) high-very high risk.

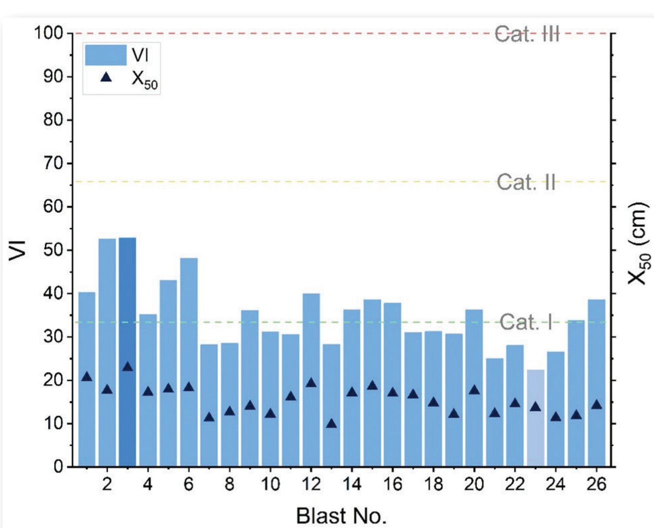


**Fig. 2** Relationship between vulnerability index (VI) and mean fragment size ($X_{50}$).

## Results

Analysis of the 26 training blasts revealed that the VI ranged from approximately 22 to 53, indicating that most blasting events fall within the medium to high fragmentation risk levels (Fig. 2). The overall average vulnerability index was 35.25, which corresponds to category 2 (medium-high risk).

A regression relationship between the VI and mean fragment size was developed, allowing fragmentation outcomes to be predicted directly from the VI.

The RES model achieved a coefficient of determination of $R^2 = 0.81$, indicating strong agreement between predicted and measured fragmentation values. In comparison, the ANFIS model produced a lower $R^2$ value of 0.44, demonstrating reduced predictive capability.

## Discussion

A key advantage of the RES methodology is integrating expert knowledge with field data. Unlike purely data-driven models that require large datasets, RES incorporates engineering judgment through the interaction matrix. This allows the model to capture causal relationships between parameters that may not be evident through statistical analysis alone.

Sensitivity analysis was conducted using the cosine amplitude method (CAM) to identify the most influential parameters affecting fragmentation. The analysis showed that burden (B) and GSI had the strongest influence on mean fragment size. These parameters directly control explosive energy distribution and rock mass response during blasting. Another parameter showing significant influence was the stemming height-to-burden ratio ($S_T/B$), which exhibited strong local sensitivity. This indicates that small changes in stemming conditions may significantly affect fragmentation outcomes.

The superior performance of the RES model compared with ANFIS highlights the importance of incorporating system-level interactions when analyzing complex blasting processes.

## Conclusions

This study presents a novel VI-based RES framework for assessing fragmentation risk and predicting mean fragment size in surface mining blasts. The major conclusions of the study include:

- The RES-based vulnerability index successfully categorizes blasts according to fragmentation risk levels.
- The overall vulnerability index of 35.25 indicates medium-high fragmentation risk in the studied blasting operations.
- The RES model demonstrated superior predictive performance ($R^2 = 0.81$) compared with the ANFIS model.
- Sensitivity analysis identified burden and GSI as the most influential parameters, while the stemming-to-burden ratio exhibited strong local effects.

The framework provides a practical decision-support tool for blast design evaluation. By identifying potential fragmentation risks and optimizing blasting parameters, the method can help reduce oversized rock fragments, improve crusher efficiency and enhance overall mining productivity.

## References

A list of all references is available in the full paper.

Selected Abstract

# Electrochemical iron recovery from biologically produced magnetite via iron oxide/hydroxide conversion: First steps toward terrestrial and Martian applications

**Reza Fayaz[1,5,6], Antoine Carissimo[3,5,6], Md Izzuddin Jundullah Hanafi[4,5], Guillaume Pillot[3,5,6], Michael Baune[1,6], Thorsten M. Gesing[4,5], Sven Kerzenmacher[3,5,6], Fabio La Mantia[2,5,6] and Jorg Thöming[1,5,6,*]**

[1]Chemical Process Engineering Group (CVT), University of Bremen, Bremen, Germany
[2]Energy Storage and Conversion Systems, University of Bremen, Bremen, Germany
[3]Environmental Process Engineering Group (UVT), University of Bremen, Bremen, Germany
[4]Institute of Inorganic Chemistry and Crystallography, University of Bremen, Bremen, Germany
[5]MAPEX Center for Materials and Processes, University of Bremen, Bremen, Germany
[6]Center for Environmental Research and Sustainable Technology (UFT), University of Bremen, Bremen, Germany
*Corresponding author email: thoeming@uni-bremen.de

**Full-text paper:**
Mining, Metallurgy & Exploration (2026) 43:389–402, https://doi.org/10.1007/s42461-025-01433-8

**Keywords:** Iron production, Biomineralization, Electrochemical reduction, Low-grade ore beneficiation, Extraterrestrial mining, In situ resource utilization (ISRU)

*Ferrihydrite ($Fe^{10}O_{14}(OH)_2$), an iron oxide/hydroxide, is found in a variety of terrestrial and extraterrestrial environments. This study presents a novel approach that combines biomineralization and electrolysis for the efficient mining of low-grade iron resources. Iron-reducing* Carboxydothermus ferrireducens *bacteria converted an iron oxide/hydroxide Fe(III) mixture to magnetite. This ferrimagnetic phase was magnetically extracted and subsequently electrolyzed at 363 K in an alkaline medium to produce metallic iron. Integrating a heat treatment step increased the iron yield to 67 percent. This resulted in a high current efficiency of 63 percent and an energy consumption of 19.1 MJ/kg, which is competitive with current pyrometallurgical practices. Heat-induced morphological and chemical changes facilitated iron reduction and suppressed parasitic hydrogen evolution. Furthermore, improved reducibility of the biomineralized material was observed. This method could facilitate the exploitation of marginal iron reserves, particularly in areas where no rich ores are available. The process also promises adaptation to extraterrestrial sources such as the Martian regolith.* ■